Eur. Phys. J. A **24**, 259–274 (2005)
DOI 10.1140/epja/i2004-10144-3

THE EUROPEAN PHYSICAL JOURNAL A

Gamma-ray spectroscopy in ^{110}Sn and ^{111}Sn

M. Wolińska-Cichocka[1,2], J. Kownacki[1,a], W. Urban[2], E. Ruchowska[3], W.A. Płóciennik[3], B. Bekman[4], Ch. Droste[2], W. Gast[5], R. Lieder[5], W. Męczyński[6], M. Kisieliński[1,3], A. Kordyasz[1], M. Kowalczyk[1,2], P. Kowina[4], J. Iwanicki[1], T. Morek[2], J. Perkowski[7], J. Srebrny[2], A. Stolarz[1], and J. Styczeń[6]

[1] Heavy Ion Laboratory, Warsaw University, Pasteura 5A, 02-093 Warszawa, Poland
[2] Faculty of Physics, Warsaw University, Hoża 69, 00-681 Warszawa, Poland
[3] The Andrzej Sołtan Institute for Nuclear Studies, Świerk, PL-05-400 Otwock-Świerk, Poland
[4] Department of Physics, Silesia University, Katowice, Poland
[5] Institut für Kernphysik, Forschungszentrum, Jülich, D-52425 Jülich, Germany
[6] The H. Niewodniczański Institute of Nuclear Physics, 31-342 Kraków, Poland,
[7] Department of Physics, University of Łódź, ul. Pomorska 149/153, 90-286 Łódź, Poland

Received: 9 August 2004 / Revised version: 18 February 2005 /
Published online: 19 April 2005 –
Communicated by W. Henning

Abstract. Excited states in ^{110}Sn and ^{111}Sn nuclei have been investigated using in-beam γ-ray spectroscopic methods. An ^{16}O beam with an energy of 60–80 MeV was used to bombard a ^{98}Mo target. On the basis of the relative excitation functions, γ-ray angular distributions, γ-γ and γ-time distributions, γ-ray multiplicity and total energy data, the level schemes of ^{110}Sn and ^{111}Sn have been studied and extended up to $E_{\rm exc} \sim 11.5$ MeV, $I = 24\hbar$, and $E_{\rm exc} \sim 11.1$ MeV and $I = (51/2)\hbar$, respectively. An extension of the intruder, g.s. and negative-parity bands, as well as 5 new band-like structures are proposed in ^{110}Sn. The nature of newly introduced collective band 8 as well as 10^+ states fed in the decay of the collective band is discussed. In the ^{111}Sn nucleus an intruder band based on the $23/2^-$ state has been reinvestigated and the extension of the g.s. band and second negative-parity band is given. Evidence for neutron-core coupling in ^{111}Sn is found. The structure and systematics of excited states in light Sn isotopes is discussed.

PACS. 27.60.+j $90 \leq A \leq 149$ – 23.20.Lv γ transitions and level energies – 21.60.Cs Shell model – 21.10.Re Collective levels

1 Introduction

The neutron shell $N = 50$–82 contains the positive-parity $s_{1/2}$, $d_{3/2}$, $d_{5/2}$ and $g_{7/2}$, and the unique-parity high-j $h_{11/2}$ orbitals. At the beginning of the shell, the ground state of nuclei is formed by the $d_{5/2}$ orbital and in ^{111}Sn it shifts to the $g_{7/2}$ configuration. Hence, the low-energy part of the ^{110}Sn level scheme is expected to be dominated by the neutron $d_{5/2}$ and $g_{7/2}$ excitations. Spherical states in this part of the level scheme are interpreted as pure neutron configurations, while at higher energies the deformed "particle-hole intruding" excitations across the proton closed $Z = 50$ shell become important. Excitations of this type are expected to deform nuclei and to generate rotational bands [1].

The low-spin states in ^{110}Sn have previously been investigated in the ^{110}Sb decay [2] as well as in a number of reaction studies [3–6], where the existence of the 5.6 ns, 6^+ isomer decaying through the 280, 985 and 1212 keV transitions has been well proven. The odd-A tin and antimony isotopes have been of interest because of intruder bands observed in ^{111}Sn and ^{109,113}Sb [7,8]. Excited states of the ^{111}Sn nucleus were previously investigated in a β-decay of ^{111}Sb [9] as well as in in-beam experiments including both single nucleon transfer [10] and heavy-ion reactions [7].

There are, however, still several reasons for the investigation of light Sn nuclei:
1) Rotational bands proposed to be built on proton 2p-2h excitations have been observed in the $^{116-118}$Sn even-mass nuclei down to the 0^+ band heads [4], whereas in ^{110}Sn and ^{112}Sn no intruder band members below spin $10\hbar$ were observed [5,6]. The odd-mass Sn nuclei, like ^{111}Sn, are believed to have a rotational band constructed of the valence neutron coupled to the 2p-2h intruder states in even-even Sn nuclei. It is important to show the presence of enhanced intraband $B(E2)$ values as well as hindered or much reduced interband decays [11] in order to give reasons for shape coexsistence in these nuclei.

[a] e-mail: jko@slcj.uw.edu.pl

2) Regular level energy systematics of excited states in even Sn nuclei breaks in the case of ^{110}Sn.
3) Several states are "missing", *e.g.* the $10_2^+, 3^-, 5^-$ states, and several low-spin members of the negative-parity and intruder bands are not known.
4) Studies of the middle- and high-spin states in ^{111}Sn could yield additional information on side bands, particle-core coupling and on the existence of high-spin isomeric states.
In this paper the main interest is focused on the structure of ^{110}Sn *and* ^{111}Sn *isotopes.*
The spectroscopic studies have been performed with the aim to gather more information on the intruder and side bands and their systematic behaviour as well as to resolve some ambiguities concerning level schemes of these nuclei. Preliminary results of these study have been published in refs. [12,13].

2 Experimental procedure and the results

The experimental information presented in this paper results from measurements performed at the Heavy Ion Laboratory cyclotron of the Warsaw University. Enriched ^{98}Mo targets with a thickness of 3–5.6 mg/cm^2 were bombarded with ^{16}O beam at four energies: 60, 70, 75 and 80 MeV. The beam was formed into bunches consisting of many short ($\sim$ 70 ns) cyclotron beam pulses. The duration of the bunches was adjustable and changed from 1.5 to 3 ms (repeated every 6 ms) in different runs. The beam energies were determined from the radio-frequency of the cyclotron and using TOF techniques, which implied an accuracy of $\sim$ 0.5 MeV.

The relative yield for the reaction channels leading to doubly even final nuclei was deduced from the γ-ray yields for the $2^+ \rightarrow 0^+$ transitions on the assumption that the side-feeding to the ground state could be neglected. The relative yield for the channels leading to odd-A or odd-odd final nuclei was assumed to correspond to the sum intensities of all known transitions leading to the ground state. The compound nucleus ^{114}Sn favoured the evaporation of neutrons, hence 3n and 4n reaction channels were expected to be the strongest reaction channels. However, yields of the p2n, p3n and α evaporation channels were also relatively strong at the 80 MeV bombarding energy (see table 1). The value of relative yield of 2n2p (α) channel includes also a contribution due to the radioactive decay of ^{110}In (4.9 h and 69.1 m) feeding the low-spin states of ^{110}Cd nuclei observed strongly in the γ-ray spectra measured between the beam bursts.

The OSIRIS-II array consisting of 10 Compton-suppressed HPGe detectors combined with a 48-elements BGO sum-energy and multiplicity filter was used in the measurements. The HPGe detectors were located behind the filter, and the BGO crystals served as collimators for them. The Ge detectors were placed in two rings; in the first one at angles $\Theta = \pm 38°, 87°, 90°, \pm 142°$ and in the second one at $\Theta = 25°, 63°, 117°, 155°$ with respect to the beam direction. Relative excitation functions, γ-ray angular distributions, linear polarization data (ref. [12]), as well as prompt and delayed (in millisecond and nanosecond regions) γ-ray singles and $\gamma\gamma$ coincidence spectra have been measured.

Table 1. Relative yields for channels observed in the ^{16}O (80 MeV) + ^{98}Mo reaction. Below each symbol of the final nucleus the pertinent reaction channel is followed by the respective relative yield. Those yields are given as a percentage of the total reaction yield evaluated from intensities of γ-lines leading to the ground state of the final nucleus in each reaction channel.

$N\backslash Z$	**60**	**61**	**62**	**63**	**64**
50	^{110}Sn 4n **18.4(5)**	^{111}Sn 3n **17.8(4)**	^{112}Sn 2n **2.9(9)**	^{113}Sn n **< 0.2**	^{114}Sn *CN*
49	^{109}In p4n **1.2(9)**	^{110}In p3n **5.2(20)**	^{111}In p2n **8.1(5)**	^{112}In np **< 0.2**	^{113}In p
48	^{108}Cd 2p4n **6.2(5)**	^{109}Cd 2p3n **0.7(6)**	^{110}Cd 2p2n **33.0(3)**	^{111}Cd 2pn **4.2(5)**	^{112}Cd 2p
47	^{107}Ag 3p4n **< 0.2**	^{108}Ag 3p3n **0.8(7)**	^{109}Ag 3p2n **< 0.2**	^{110}Ag 3pn **0.9(8)**	^{111}Ag 3p

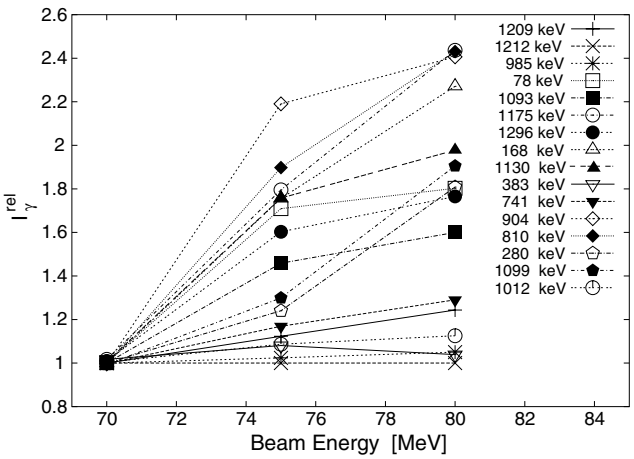

Fig. 1. Relative excitation functions determined for selected γ-rays from the ^{98}Mo(^{16}O, 4nγ)^{110}Sn reaction.

The isotopic assignment of γ-rays following the ^{98}Mo(^{16}O, xnyp) reaction was supported by the behaviour of their yields as a function of the bombarding energy. Examples of relative excitation functions measured for the most prominent γ-rays assigned to the 4n and 3n reaction channels are shown in figs. 1 and 2. The relative excitation functions for the γ-rays depopulating non-yrast levels exhibit usually a pattern, which differs from that of the yrast states. Quite pronounced differences occur for low-spin non-yrast levels, when compared to the yrast states with the corresponding spin. The 810 and 904 keV γ-rays from the cascade feeding the 10^+, 5227 keV yrast state in ^{110}Sn have clearly the steepest relative excitation functions, suggesting relatively high spins of their initial levels. Similarly, the relative excitation functions of 768,

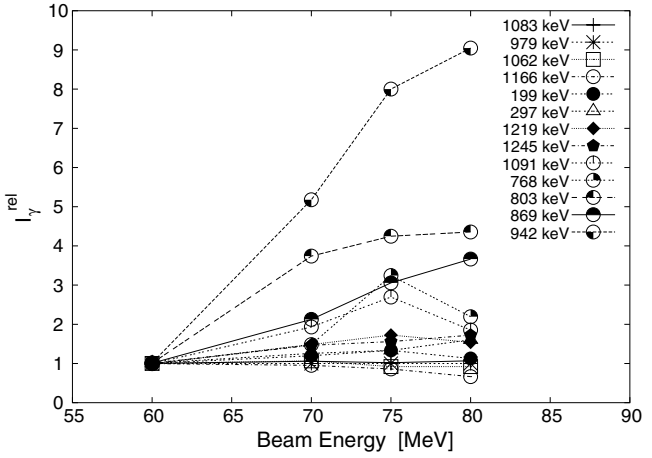

Fig. 2. Examples of relative excitation functions for selected γ-rays from the ^{98}Mo(^{16}O, 3nγ)^{111}Sn reaction.

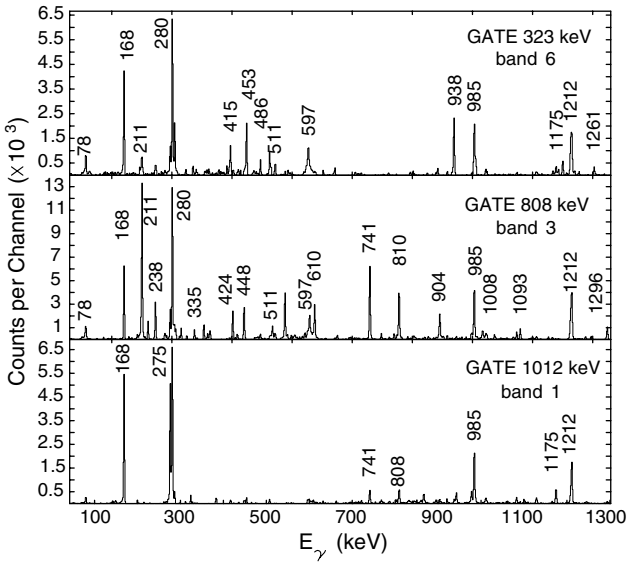

Fig. 3. Examples of coincidence spectra obtained in the ^{98}Mo(^{16}O, 4nγ) reaction at a bombarding energy of 80 MeV. Representative gates for possible continuation (band 6) of the ground-state band, intruder band (3), and negative-parity band (1) in ^{110}Sn are selected. The 938 keV γ-ray (which might be ascribed to the ^{110}Cd and ^{108}Ag nuclei) is observed in the 323 keV gate due to the presence of α (^{110}Cd), α2n (^{108}Cd) and αpn (^{108}Ag) reaction channels.

803, 869, 942 and 1091 keV γ-rays in ^{111}Sn (fig. 2) show the slopes indicating that they are emitted from states with rather high spins.

A total of $\sim 10^8$ events were recorded in the $\gamma\gamma$ coincidence measurements. The data were sorted off-line into several $\gamma\gamma$ matrices with various time conditions (prompt and off-beam with several time windows) and various combinations of detector angles. Specific conditions were put on multiplicity and total energy in order to enhance the desired reaction channel. The analysis of $\gamma\gamma$ matrices and construction of the level schemes was performed using the RadWare software package [14].

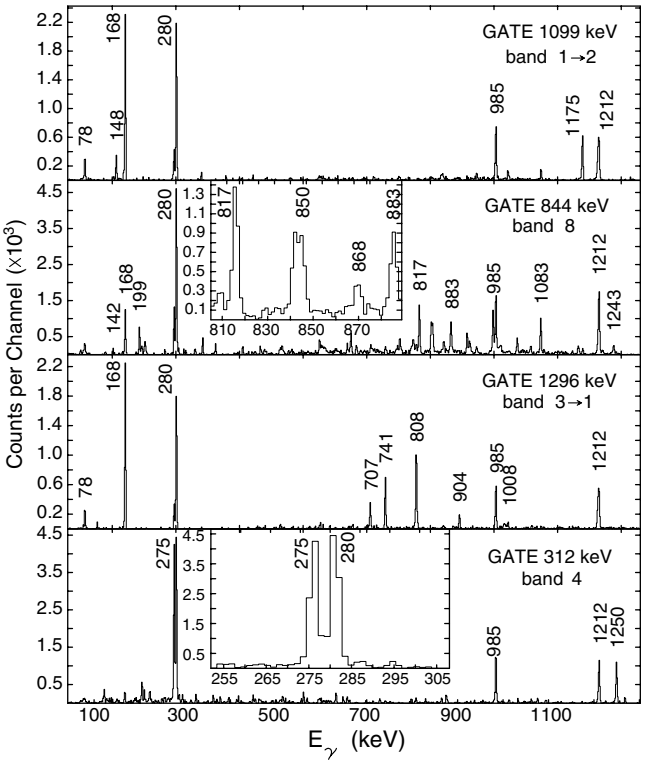

Fig. 4. Examples of $\gamma\gamma$ coincidence spectra for ^{110}Sn gated on the 312 keV transition in band 4, $(8^+) \rightarrow (7^+)$, 1296 keV transition illustrating the connection of band 3 with negative-parity band 1, 844 keV transition showing the coincidence relations in band 8, and 1099 keV transition showing a link of band 1 and band 2 as observed in the ^{98}Mo(^{16}O, 4nγ) reaction at 80 MeV bombarding energy.

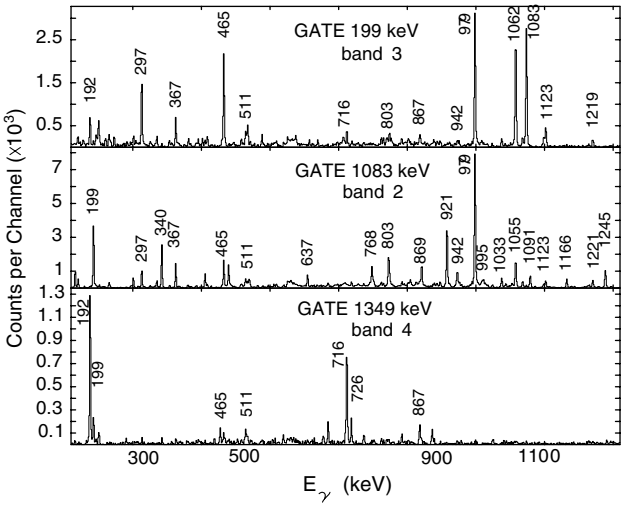

Fig. 5. The background-corrected, $\gamma\gamma$ coincidence spectra for bands in ^{111}Sn populated in the ^{98}Mo(^{16}O, 3nγ) reaction at 80 MeV.

Examples of the coincidence spectra illustrating the main features of the level schemes are shown in figs. 3 and 4 for ^{110}Sn and in figs. 5 and 6 for ^{111}Sn.

The conventional angular-distribution measurements were performed at six different angles with respect to the

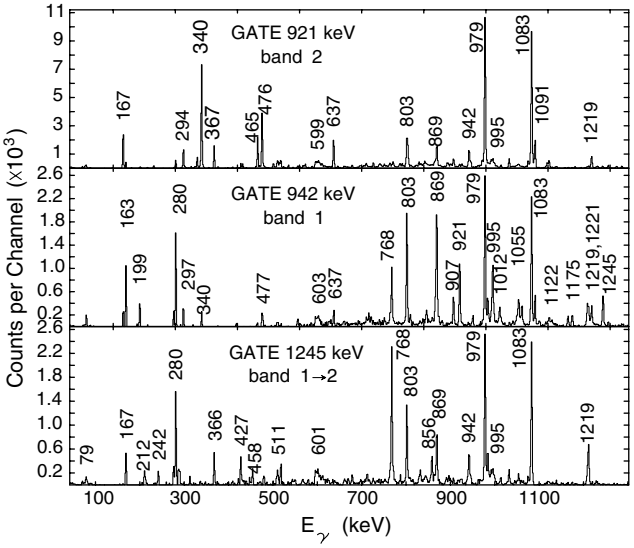

Fig. 6. Background-corrected, coincidence spectra obtained for ^{111}Sn in the ^{98}Mo(^{16}O, 3n) reaction. Spectra gated by the 942 keV and 1245 keV transitions demonstrate the higher-spin part of the intruder band, while the spectrum gated on the 921 keV line shows lines from bands 1, 2 and 3.

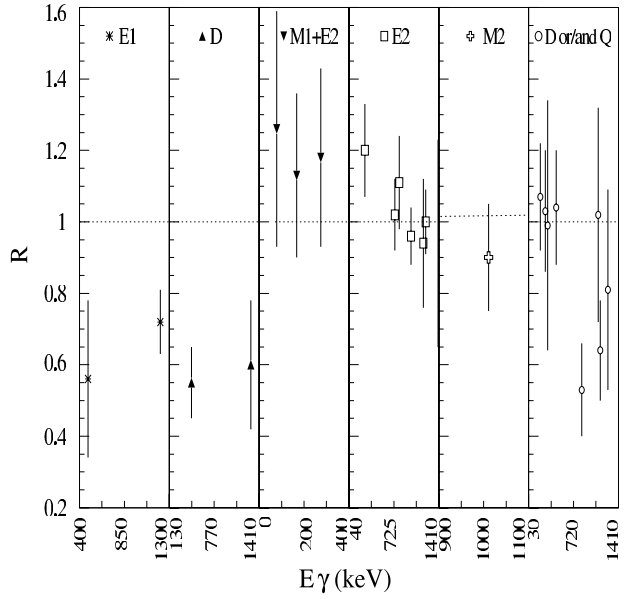

Fig. 7. DCO ratios determined for selected γ-rays from the ^{98}Mo(^{16}O, xn) reaction.

beam axis. The data were normalized to transitions with isotropic angular distributions from the radioactivity spectrum and corrected for the efficiency of individual detectors. Subsequently, the resulting intensities were normalized to those observed at 90°. The $\gamma\gamma$ matrices sorted for different combinations of detector angles were used to investigate angular correlations between the emitted γ-rays. The multipolarities of new γ-transitions were also derived from $R_{\rm DCO}$ ratios defined as

$$R_{\rm DCO} = \frac{I_\gamma(E_\gamma; 38^\circ + 25^\circ)}{I_\gamma(E_\gamma; 90^\circ + 87^\circ)} \,. \qquad (1)$$

In order to determine the $R_{\rm DCO}$ ratios, the data were sorted into E_γ-E_γ matrices with the following angle combinations: i) $(38^\circ + 25^\circ)$ *vs.* all angles and ii) $(90^\circ + 87^\circ)$ *vs.* all angles, where first the x-axis and then the y-axis is given. By setting identical gates on the desired γ-rays in both matrices, coincidence spectra were created from which the intensity ratio $R(E_\gamma)$ could be extracted. To make the spin-parity assignments, it was assumed that the observed transitions were of $E1$, $M1$ or $E2$ type. The obtained ratios have values around 0.6 or 1.0 (fig. 7). The first value corresponds to dipole $\Delta I = 1$ transitions, while the second to stretched quadrupole $\Delta I = 2$, and non-stretched $\Delta I = 0$ dipole transitions. In many cases, the same state is reached via various decay paths, which helps to resolve ambiguities.

3 The level schemes

3.1 The nucleus ^{110}Sn

The level scheme based on the data obtained in the ^{98}Mo(^{16}O, 4nγ)^{110}Sn reaction is shown in fig. 8 where eight band-like structures are presented. The γ-rays assigned to ^{110}Sn together with their relative intensities, angular-distribution coefficients and DCO ratios as well as spins and parities proposed for the initial and final states are listed in table 2. Part of the level scheme up to the 6^+, ~ 5.6 ns, 2477 keV isomer (band 5), and band 3 up to the 20^+, ~ 9.5 MeV state were already known from earlier experiments [3–6].

3.1.1 Band 5. The 1212, 2197, 2477 keV levels

The γ-ray cascades displayed in fig. 8 proceed through the positive- and negative-parity states and feed mainly the lowest 2^+, 4^+ and 6^+ states with energies of 1212, 2197 and 2477 keV, respectively. These states are de-excited by the three most intense γ-rays observed in the ^{98}Mo(^{16}O, 4nγ)^{110}Sn reaction which have energies 1212, 985 and 280 keV and constitute a stretched $E2$ yrast cascade. This assignment is strongly confirmed in the present work by the relative excitation functions, coincidence results, angular distributions, lifetime estimates and DCO ratios.

3.1.2 Band 1

The existence of a low-lying 3^- state at an energy of 2458 keV was suggested in a ^{112}Sn(p, t) reaction study [15]. In the present work, the 3^- state is confirmed at an energy of 2458 keV, as a coincidence was observed between the new 1246 keV γ-ray and the 1212 keV, $2^+ \rightarrow 0^+$ transition, and with the 896 keV transition de-exciting the 3354 keV, as suggested (5^-) level. A candidate for another 5^- state is also the 2963 keV level connected with the 6^+, 2477 keV state by the 486 keV γ-ray showing a strong negative anisotropy, $A_2/A_0 = -0.44$

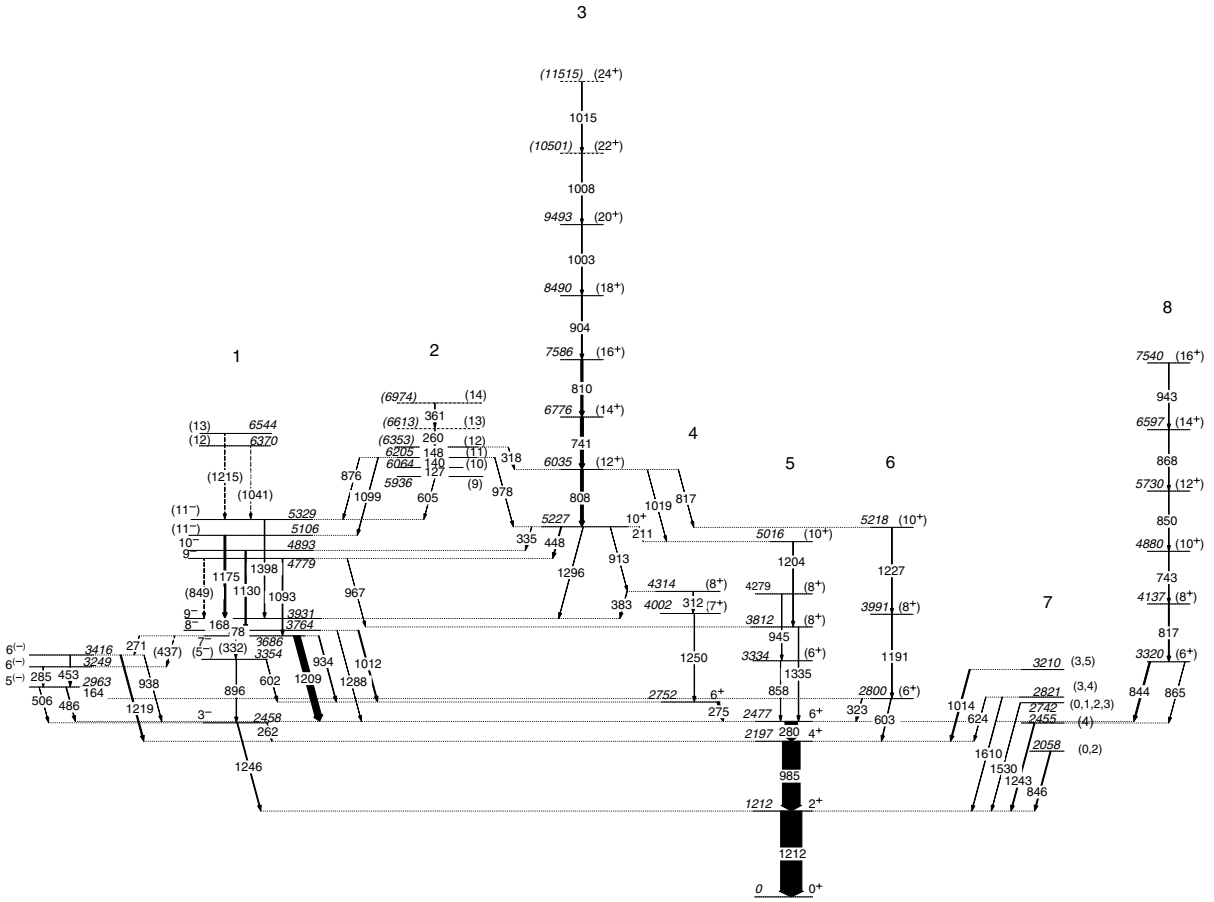

Fig. 8. The level scheme of ^{110}Sn, as observed in the ^{98}Mo(^{16}O, 4nγ) reaction.

and $A_4/A_0 = 0.01$, consistent with expectations for a $5^- \rightarrow 6^+$, $E1$ transition. The 453 keV γ-ray observed in coincidence with the 486 keV transition de-excites a new level introduced at 3416 keV. The 453 keV γ-ray is probably of dipole, $M1$ character, with a significant admixture of the $E2$ component, suggesting a $6^{(-)}$ spin-parity assignment for the 3416 keV level. The observation of γ-transitions linking the 3416 keV level with the 3^-, 2458 keV and 7^-, 3686 keV states additionally supports both the placement and spin-parity assignments of the 2963 keV and 3416 keV levels.

The 3249 keV level

The 3249 keV level was introduced in the (p, t) reaction study [15] with an $l = 4$ assignment; however, no γ-rays feeding or de-exciting this level were known. In the present study, the energy of 3249 keV is determined for this level by observing a new 285 keV transition connecting this state with the $5^{(-)}$, 2963 keV level. Because of its negative anisotropy this transition can be classified as a mixed dipole-quadrupole transition, suggesting a spin assignment $I = 5$ or 6 for the 3249 keV level. The observation of a weak coincidence of the 285 keV γ-ray with the 437 keV one de-exciting the 7^-, 3686 keV state is in favour of the $I = 6$ assignment.

The 7^-, 3686 keV, 8^-, 3764 keV and 9^-, 3931 keV levels

These levels are confirmed in the present study due to the observation of the 934 keV and 1209 keV transitions of dipole, most probable $E1$ character, de-exciting the 3686 keV state. Besides, three new γ-rays of energies 271, 332 and 437 keV de-exciting the 3686 keV state were also observed.

The 4779, 4893, 5106 and 5329 keV levels

The 4779 keV level de-excites through the 1093 keV transition of quadrupole, most probably of $E2$ character according to angular-distribution results, feeding the 7^-, 3686 keV level. This suggests a 9^- spin-parity assignment for this level. The observation of a 448 keV γ-ray linking this level with the 10^+, 5227 keV level and of weak 849 and 967 keV transitions depopulating this level gives further support for the 9^- assignment. The 4893, 5106 and 5329 keV levels are de-excited via the 1130, 1175 and 1398 keV γ-rays, respectively. The 6370 keV and 6544 keV levels introduced here are based on the coincidence relations of 1041 and 1215 keV γ-rays, and are candidates for the $12^{(-)}$ and $13^{(-)}$ states. However, no definite conclusions concerning the parity assignments for these two levels have been obtained.

Table 2. Gamma-ray transitions assigned to ^{110}Sn. Gamma-ray energies (E_γ), excitation energies (E_i) of the initial level, relative γ-ray intensities, angular-correlations ratios R_DCO, angular-distribution coefficients, as well as the proposed spin and parity assignments are given.

E_γ (keV)	E_i (keV)	I_γ (relative)	R_DCO	$W(\theta)$ A_2/A_0	A_4/A_0	$J_\mathrm{i}^\pi \rightarrow J_\mathrm{f}^\pi$ ($\hbar$)
78.3(0.1)	3764	13.8(5)	1.26(33)	0.07(5)	0.06(3)	$8^- \rightarrow 7^-$
127.0(0.1)	6064	0.3(2)	–	–	–	$(10) \rightarrow (9)$
140.2(0.2)	6205	0.2(0)	–	–	–	$(11) \rightarrow (10)$
147.7(0.3)	6353	0.3(0)	–	–	–	$(12) \rightarrow (11)$
163.9(0.1)	2963	0.9(1)	–	–	–	$5^- \rightarrow (6^+)$
167.5(0.1)	3931	12.7(4)	1.13(23)	–	–	$9^- \rightarrow 8^-$
211.0(0.2)	5227	0.8(0)	1.07(15)	−0.15(1)	−0.20(22)	$10^+ \rightarrow (10^+)$
259.6(0.5)	6613	0.3(0)	–	–	–	$(13) \rightarrow (12)$
261.5(0.2)	2458	1.9(2)	–	–	–	$3^- \rightarrow 4^+$
270.8(0.2)	3686	1.8(1)	–	–	–	$7^- \rightarrow 6-$
275.3(0.4)	2752	10.3(3)	1.18(25)	0.35(9)	−0.01(2)	$6^+ \rightarrow 6^+$
280.2(0.3)	2477	57(2)	1.20(13)	0.11(1)	−0.14(9)	$6^+ \rightarrow 4^+$
285.4(0.7)	3249	2.0(3)	1.03(17)	−0.13(19)	0.04(7)	$6^- \rightarrow 5^-$
311.7(0.2)	4314	1.1(1)	–	0.25(21)	0.02(2)	$(8^+) \rightarrow (7^+)$
318.0(8.0)	6353	0.1(1)	–	–	–	$(12) \rightarrow (12^+)$
323.1(0.1)	2800	2.8(2)	–	–	–	$(6^+) \rightarrow 6^+$
332.0(0.1)	3686	0.2(1)	–	–	–	$7^- \rightarrow (5^-)$
334.5(0.3)	5227	0.5(0)	–	–	–	$10^+ \rightarrow 10^-$
361.2(1.0)	6974	0.1(1)	–	–	–	$(14) \rightarrow (13)$
382.7(0.4)	4314	0.5(1)	–	–	–	$(8^+) \rightarrow 9^-$
437.2(0.3)	3686	0.7(1)	–	–	–	$7^- \rightarrow (5,6)$
447.7(0.8)	5227	3.4(1)	0.55(10)	−0.35(16)	0.001(3)	$10^+ \rightarrow 9^-$
453.4(0.1)	3416	1.4(3)	1.04(16)	0.36(20)	0.06(9)	$6^- \rightarrow 5^-$
486.0(0.1)	2963	1.3(1)	0.56(22)	−0.44(14)	0.01(2)	$5^- \rightarrow 6^+$
505.8(0.2)	2963	1.1(1)	–	–	–	$5^- \rightarrow 3^-$
602.1(0.3)	3354	1.5(1)	–	–	–	$(5^-) \rightarrow 6^+$
603.4(0.1)	2800	5.9(5)	–	–	–	$(6^+) \rightarrow 4^+$
604.5(0.6)	5936	≤0.1	–	–	–	$(9) \rightarrow (11^-)$
624.0(0.9)	2821	0.8(4)	–	–	–	$(2,3,4,5) \rightarrow 4^+$
740.9(0.1)	6776	9.7(4)	1.02(10)	0.29(9)	−0.06(7)	$(14^+) \rightarrow (12^+)$
743.2(0.1)	4880	3.2(3)	–	–	–	$(10^+) \rightarrow (8^+)$
808.2(0.1)	6035	9.8(6)	1.11(13)	0.43(10)	−0.01(1)	$(12^+) \rightarrow 10^+$
809.9(0.1)	7586	10.4(5)	1.11(13)	0.43(11)	−0.01(1)	$(16^+) \rightarrow (14^+)$
816.7(0.1)	4137	4.4(3)	–	–	–	$(8^+) \rightarrow 6^+$
816.9(0.4)	6035	0.8(1)	–	–	–	$(12^+) \rightarrow (10^+)$
843.5(0.1)	3320	4.7(4)	0.53(13)	–	–	$(6^+) \rightarrow 6^+$
846.0(0.4)	2058	4.6(1)	–	–	–	$(0,2) \rightarrow 2^+$
848.5(0.9)	4779	0.2(1)	–	–	–	$9^- \rightarrow 9^-$
849.7(0.2)	5730	1.4(2)	–	–	–	$(12^+) \rightarrow (10^+)$
857.5(0.4)	3334	1.2(3)	–	–	–	$(6^+) \rightarrow 6^+$
865.0(0.5)	3320	1.2(2)	–	–	–	$(6^+) \rightarrow (4)$
867.5(0.2)	6597	1.3(1)	–	–	–	$(14^+) \rightarrow (12^+)$
876.0(0.4)	6205	0.8(1)	–	–	–	$(11) \rightarrow (11^-)$
896.2(0.3)	3354	2.3(3)	–	–	–	$(5^-) \rightarrow 3^-$
903.9(0.1)	8490	4.2(0)	–	0.17(17)	−0.10(16)	$(18^+) \rightarrow (16^+)$
912.8(0.7)	5227	0.3(0)	–	–	–	$10^+ \rightarrow (8^+)$
933.9(0.2)	3686	1.7(1)	–	−0.22(9)	0.01(1)	$7^- \rightarrow 6^+$
938.3(0.3)	3416	1.8(3)	–	–	–	$6^- \rightarrow 6^+$
942.8(0.2)	7540	1.6(1)	–	–	–	$(16^+) \rightarrow (14^+)$
945.4(0.5)	4279	0.8(2)	–	–	–	$(8^+) \rightarrow (6^+)$
967.4(0.4)	4779	0.3(1)	–	–	–	$9^- \rightarrow (8^+)$
978.2(0.1)	6205	1.3(4)	–	–	–	$(11) \rightarrow 10^+$
984.6(0.4)	2197	83(3)	0.96(08)	0.29(7)	−0.01(1)	$4^+ \rightarrow 2^+$
1003.3(0.1)	9493	2.7(2)	–	–	–	$(20^+) \rightarrow (18^+)$
1007.6(0.2)	10501	1.3(1)	–	–	–	$(22^+) \rightarrow (20^+)$

Table 2. Continued.

E_γ (keV)	E_i (keV)	I_γ (relative)	R_DCO	$W(\theta)$ A_2/A_0	$W(\theta)$ A_4/A_0	$J^\pi_\mathrm{i} \to J^\pi_\mathrm{f}$ ($\hbar$)
1012.3(0.1)	3764	5.2(3)	0.90(15)	0.30(12)	−0.06(7)	$8^- \to 6^+$
1013.8(0.3)	3210	4.0(6)	–	J=3: 0.15(20) J=5: 0.15(20)	J=3: 0.003(7) J=5: 0.01(2)	(3,5)→4+
1014.5(0.2)	11515	1.3(1)	–	–	–	$(24^+) \to (22^+)$
1019.1(0.9)	6035	0.4(1)	–	–	–	$(12^+) \to (10^+)$
1041.0(1.0)	6370	0.3(1)	–	–	–	$(12) \to (11^-)$
1092.9(0.1)	4779	3.6(3)	–	0.24(11)	−0.09(5)	$9^- \to 7^-$
1099.0(0.1)	6205	2.5(1)	0.90(15)	–	–	$(11) \to (11^-)$
1129.5(0.1)	4893	6.1(3)	0.64(14)	0.26(11)	−0.08(7)	$10^- \to 8^-$
1175.3(0.5)	5106	8.9(3)	0.94(18)	0.33(8)	−0.05(2)	$(11^-) \to 9^-$
1191.1(0.3)	3991	1.9(3)	–	–	–	$(8^+) \to (6^+)$
1203.7(0.2)	5016	2.1(2)	–	–	–	$(10^+) \to (8^+)$
1208.8(0.5)	3686	31(1)	0.72(09)	−0.29(9)	0.01(1)	$7^- \to 6^+$
1211.8(0.4)	1212	100(8)	1.00(09)	0.20(7)	−0.07(4)	$2^+ \to 0^+$
1215.3(0.1)	6544	1.4(2)	–	–	–	$(13) \to (11^-)$
1219.3(0.2)	3416	6.0(5)	–	–	–	$6^{(-)} \to 4^+$
1227.4(0.4)	5218	0.7(1)	–	–	–	$(10^+) \to (8^+)$
1242.5(0.8)	2455	1.7(7)	–	–	–	$(4) \to 2^+$
1246.4(0.2)	2458	4.8(6)	–	−0.16(5)	0.01(2)	$3^- \to 2^+$
1249.9(0.2)	4002	2.1(2)	0.81(28)	0.47(37)	0.13(10)	$(7^+) \to 6^+$
1287.5(0.5)	3764	0.9(1)	–	–	–	$8^- \to 6^+$
1295.6(0.1)	5227	1.9(1)	0.60(18)	0.40(36)	0.16(18)	$10^+ \to 9^-$
1335.0(0.1)	3812	2.3(2)	–	0.36(15)	−0.03(4)	$(8^+) \to 6^+$
1397.6(0.1)	5329	2.7(1)	0.94(29)	0.19(8)	−0.11(6)	$(11^-) \to 9^-$
1530.1(0.8)	2742	1.7(5)	–	–	–	(0,1,2,3)→2+
1609.8(0.6)	2821	2.3(6)	–	J=3: 0.10(10) J=4: 0.06(6)	J=3: 0.01(1) J=4: −0.15(15)	(3,4)→2+

Table 3. Experimental $B(E2)$, γ-ray branching ratios (λ) obtained in this work in light Sn isotopes. Subscripts i and y denote intraband and interband transitions (to the yrast or side bands), respectively. Intensities I_γ are given with reference to the 1212 keV (^{110}Sn), 979 keV (^{111}Sn) and 1257 keV (^{112}Sn) γ-rays, respectively.

$^A X$	$E_x^\mathrm{init.lev.}$ (keV)	E_γ (keV)	I_i	I_f	I_γ	$\lambda = \frac{i\to i}{i\to y}$	$K_\mathrm{exp} = \frac{B(E2)_\mathrm{intraband}}{B(E2)_\mathrm{interband}}$
^{110}Sn	6035	808	$(12^+)_i$	$(10^+)_i$	9.80 ± 0.70	25 ± 8	79 ± 25
		1019	$(12^+)_i$	$(10^+)_y$	0.44 ± 0.13		
	6035	808	$(12^+)_i$	$(10^+)_i$	9.80 ± 0.70	12 ± 2	12 ± 2
		817	$(12^+)_i$	$(10^+)_y$	0.80 ± 0.10		
^{111}Sn	4074	768	$(23/2^-)_i$	$(19/2^-)_i$	13.60 ± 0.70	1.1 ± 0.1	6.3 ± 0.5
		1091	$(23/2^-)_i$	$(19/2^-)_y$	12.40 ± 0.80		
	4074	768	$(23/2^-)_i$	$(19/2^-)_i$	13.60 ± 0.70	2.2 ± 0.2	6.4 ± 0.6
		951	$(23/2^-)_i$	$(19/2^-)_y$	6.20 ± 0.50		
	4074	768	$(23/2^-)_i$	$(19/2^-)_i$	13.60 ± 0.70	2.7 ± 0.1	4.3 ± 0.2
		846	$(23/2^-)_i$	$(19/2^-)_y$	5.10 ± 0.07		
	4074	1091	$(23/2^-)_i$	$(19/2^-)_i$	12.40 ± 0.80	2.0 ± 0.2	1.1 ± 0.1
		951	$(23/2^-)_i$	$(19/2^-)_y$	6.20 ± 0.50		
	5746	869	$(31/2^-)_i$	$(27/2^-)_i$	21.00 ± 1.00	4.7 ± 0.4	5.8 ± 0.5
		907	$(31/2^-)_i$	$(27/2^-)_y$	4.55 ± 0.05		
	3620	637	$(23/2^-)_i$	$(19/2^-)_i$	5.00 ± 0.50	50 ± 20	1.5 ± 0.8
		314	$(23/2^-)_i$	$(19/2^-)_y$	0.10 ± 0.20		
^{112}Sn	3416	893	$(6^+)_i$	$(4^+)_i$	1.43 ± 0.50	0.4 ± 0.2	1.7 ± 0.7
		1167	$(6^+)_i$	$(4^+)_y$	3.30 ± 0.82		
	3416	631	$(6^+)_i$	$(4^+)_i$	2.05 ± 0.64	0.6 ± 0.3	13.4 ± 5.3
		1167	$(6^+)_i$	$(4^+)_y$	3.30 ± 0.82		
	5568	745	$(12^+)_i$	$(10^+)_i$	2.86 ± 0.62	7.8 ± 3.7	19 ± 10
		888	$(12^+)_i$	$(10^+)_y$	0.36 ± 0.25		
	6367	800	$(14^+)_i$	$(12^+)_i$	5.19 ± 0.81	5.3 ± 2.5	2.4 ± 1.4
		680	$(14^+)_i$	$(12^+)_y$	0.98 ± 0.25		

3.1.3 Band 2

A new sequence of levels showing a $\Delta I = 1$ structure is observed. This band decays via weak γ-rays to band 1 and band 3. Tentative spin assignments are based on the dipole character of the 605, 876 and 1099 keV transitions. Further investigations are needed.

3.1.4 Band 3

An intruder band consisting of a cascade of the 808, 741, 810, 904 and 1003 keV γ-rays as established in [3,4] is confirmed in the present work (see fig. 3, spectrum gated on the 808 keV γ-ray). An extension of this band towards higher spins ((22^+) state de-excited by the 1008 keV γ-ray and (24^+) state de-excited by the 1015 keV γ-ray) is proposed, based on the coincidence data and intensity relations. In addition to this cascade, the transitions linking band 3 with levels belonging to bands 1, 4, 5 and 6 have been observed. In particular, the decay of the 10^+, 5227 keV level is fragmented. Also the (12^+) state at 6035 keV decays via 808, 817 and 1019 keV transitions, most probably of $E2$ character, feeding three 10^+ states.

A comparison of preliminary experimental ratios

$$K_{\rm exp} = \frac{B(E2)_{\rm intraband}}{B(E2)_{\rm interband}} \qquad (2)$$

for the intruder bands in light Sn nuclei obtained in the present work was reported in ref. [13]. The data, given in table 3, show rather strong intraband $B(E2)$ values as compared to the hindered interband decays.

3.1.5 The band-like structures 4 and 6 and the upper part of band 5 (g.s. band)

A cascade of 312, 1250 and 275 keV transitions (fig. 4) of $M1 + E2$ character (with significant admixture of $E2$), labeled in fig. 8 as band 4, is strongly connected to the g.s. band 5 via a 275 keV transition de-exciting the 6^+, 2752 keV state. Based on the angular distributions and DCO results, one can propose (7^+) and (8^+) assignments for the 4002 and 4314 keV levels, respectively. However, the 8^+ and 9^+ assignments cannot be completely ruled out. In the case of the 4314 keV level, both assignments are in agreement with an $E1$ character for the 383 keV transition linking this level with the 9^-, 3931 keV state from band 1. A second cascade, feeding the 6^+ yrast state found in this work consists of the 1227, 1191 and 323 keV transitions (band 6) starting from the 5218 keV level. The connection of this level with the (12^+), 6035 keV state of the intruder band via a weak 817 keV transition suggests a high spin for this state. A similar structure consisting of 1204 and 1335 keV transitions is placed at the top of 6_1^+ yrast state (band 5). Also in this case a weak connection (1019 keV) between the 6035 keV and 5016 keV levels is observed pointing at a high-spin assignment for the latter level. The 1204, 1335 as well as the 1227 and 1191 keV transitions having most likely a stretched $E2$ character, might suggest that the 5218 and 5016 keV levels are the missing 10^+ states we are searching for.

3.1.6 Bunch of levels labeled as band 7

The 2058, 2455, 2742, 2821 and 3210 keV levels are introduced relying on coincidence relations with the 985 and 1212 keV γ-rays from the g.s. band. Possible spin assignments are based on intensity and coincidence relations as well as on lifetime information giving the recommended upper limits for γ-ray strengths [16].

3.1.7 Band 8

A spectrum gated on the 844 keV transition (fig. 4), which has most probably $E2$ character, shows a previously unreported sequence of 817, 743, 850, 868 and 943 keV transitions. Based on the regular character of this cascade resembling the behaviour of stretched quadrupole transitions in a rotational-like band, tentative spins up to $16\hbar$ are proposed. Information concerning the multipolarities of these transitions is obscured because each of the considered peaks is placed on the tail of a close in energy strong transition.

3.2 The nucleus ^{111}Sn

The level scheme of ^{111}Sn is presented in fig. 9 and the γ-rays assigned to this nucleus are listed in table 4. Figure 5 shows evidence for the existence of positive-parity states sequence (band 4) and gives the connections of band 2 (g.s. band) with band 3 (another negative-parity band) and band 1 (intruder band). Additionally, fig. 6 displays a γ-ray spectrum gated on the 921 keV transition showing γ-rays from the g.s. band and from the two side bands, while spectra gated on the 942 and 1245 keV transitions are demonstrating the higher-spin part of the intruder band. The present investigation confirms, with a few exceptions, the levels previously found [7–10] and extends the knowledge about the low-spin part of the ^{111}Sn level scheme.

3.2.1 Band 1

An intruder band built on the $23/2^-$, 4074 keV level and decaying by the stretched quadrupole transitions has been established in previous studies [7,17]. In the present work, it was found that the decay of the 4074 keV level is very fragmented. Apart from the relatively strong 768 and 1091 keV γ-rays, it decays also through weaker 752, 846 and 951 keV transitions. Four $19/2^-$ states are populated in this decay. Branching ratios of the intra- to inter-band $E2$ transitions for the 4074 and 5746 keV levels are given in table 3.

Table 4. Gamma-ray transitions assigned to ^{111}Sn. Gamma-ray energies E_γ, excitation energies of the initial state (E_i), relative intensities I_γ, angular-correlation ratios R_DCO and angular-distribution coefficients, as well as the proposed spin and parity assignments are given.

E_γ (keV)	E_i (keV)	I_γ (relative)	R_DCO	$W(\theta)$ A_2/A_0	A_4/A_0	$J_\mathrm{i}^\pi \rightarrow J_\mathrm{f}^\pi$ ($\hbar$)
191.9(0.2)	2257	1.6(2)	–	–	–	$19/2^+ \rightarrow 15/2^+$
198.7(0.1)	3323	6.2(3)	0.51(13)	0.07(13)	0.01(1)	$21/2^- \rightarrow 19/2^-$
297.4(0.1)	3620	2.2(2)	2.33(61)	0.25(17)	0.17(41)	$23/2^- \rightarrow 21/2^-$
313.5(0.3)	3620	0.1(2)	–	–	–	$23/2^- \rightarrow 19/2^-$
339.6(0.1)	3323	6.5(4)	1.00(17)	−0.16(12)	0.18(43)	$21/2^- \rightarrow 19/2^-$
364.8(0.9)	6131	0.6(3)	–	–	–	$(31/2) \rightarrow (29/2^-)$
367.1(0.2)	4155	2.0(2)	0.86(19)	–	–	$25/2^- \rightarrow 25/2^-$
370.0(0.2)	1349	≤ 0.3	–	–	–	$11/2^- \rightarrow 11/2^-$
465.1(0.1)	3788	5.5(4)	1.01(22)	0.38(14)	−0.02(6)	$25/2^- \rightarrow 21/2^-$
475.9(0.1)	3459	5.7(6)	0.90(30)	0.22(14)	−0.10(9)	$23/2^- \rightarrow 19/2^-$
636.7(0.1)	3620	5.0(5)	–	–	–	$23/2^- \rightarrow 19/2^-$
716.4(0.2)	2065	5.0(9)	–	0.48(19)	0.04(11)	$15/2^+ \rightarrow 11/2^+$
726.0(0.6)	2983	0.4(2)	–	–	–	$19/2^- \rightarrow 17/2^+$
751.6(0.7)	4074	1.0(3)	–	–	–	$23/2^- \rightarrow 21/2^-$
767.9(0.1)	4074	13(1)	0.62(25)	0.33(11)	−0.05(4)	$23/2^- \rightarrow 19/2^-$
802.9(0.1)	4877	27 (1)	0.85(12)	0.32(93)	−0.05(3)	$27/2^- \rightarrow 23/2^-$
845.8(0.2)	4074	5.1(5)	–	–	–	$23/2^- \rightarrow 19/2^-$
866.5(0.4)	3124	1.2(2)	–	–	–	$19/2^- \rightarrow 17/2^+$
869.4(0.1)	5746	21(1)	1.08(21)	0.25(10)	−0.08(23)	$31/2^- \rightarrow 27/2^-$
889.8(0.2)	5767	3.4(4)	–	–	–	$(29/2^-) \rightarrow 27/2^-$
907.1(0.2)	5746	4.5(3)	–	–	–	$31/2^- \rightarrow 27/2^-$
914.6(0.2)	4988	5.2(6)	–	–	–	$(27/2) \rightarrow 23/2^-$
921.2(0.1)	2983	40(2)	1.54(25)	0.31(8)	−0.06(17)	$19/2^- \rightarrow 15/2^-$
927.4(0.3)	5767	2.7(3)	–	–	–	$(29/2^-) \rightarrow 27/2^-$
942.4(0.7)	6689	20(1)	0.75(17)	0.10(11)	−0.13(12)	$35/2^- \rightarrow 31/2^-$
950.8(0.2)	4074	6.2(5)	–	–	–	$23/2^- \rightarrow 19/2^-$
971.8(0.1)	3955	8.3(8)	–	–	–	$(23/2) \rightarrow 19/2^-$
978.5(0.1)	979	100(8)	1.04(10)	0.23(7)	−0.07(4)	$11/2^- \rightarrow 7/2^+$
995.3(0.9)	7684	12(7)	–	0.30(18)	−0.05(6)	$(39/2^-) \rightarrow 35/2^-$
1033.1(0.2)	4988	5.6(6)	–	–	–	$(27/2) \rightarrow (23/2)$
1054.6(0.1)	8739	7.4(5)	–	–	–	$(43/2^-) \rightarrow (39/2^-)$
1061.5(0.1)	3124	21(1)	1.05(27)	0.39(9)	−0.02(2)	$19/2^- \rightarrow 15/2^-$
1076.0(0.1)	6843	7.7(6)	–	–	–	$(31/2^-) \rightarrow (29/2^-)$
1083.4(0.1)	2062	91(4)	0.71(23)	0.11(2)	−0.07(3)	$15/2^- \rightarrow 11/2^-$
1088.6(0.5)	4877	1.5(3)	–	–	–	$27/2^- \rightarrow 25/2^-$
1090.8(0.1)	4074	12 (1)	–	–	–	$23/2^- \rightarrow 19/2^-$
1096.7(0.2)	6843	6.1(7)	–	–	–	$(31/2^-) \rightarrow 31/2^-$
1121.8(0.2)	9861	3.2(3)	–	–	–	$(47/2^-) \rightarrow (43/2^-)$
1123.3(0.2)	4446	3.6(4)	1.87(75)	–	–	$25/2^- \rightarrow 21/2^-$
1142.7(0.5)	6131	2.0(5)	–	–	–	$(31/2) \rightarrow (27/2)$
1165.8(0.1)	3228	8(1)	–	0.02(4)	−0.18(10)	$19/2^- \rightarrow 15/2^-$
1218.5(0.2)	4839	6.0(6)	–	0.004(4)	−0.18(8)	$27/2^- \rightarrow 23/2^-$
1221.3(0.3)	11082	2.1(3)	–	–	–	$(51/2^-) \rightarrow (47/2^-)$
1244.7(0.1)	3307	18(1)	0.73(29)	0.29(9)	−0.10(1)	$19/2^- \rightarrow 15/2^-$
1254.1(0.3)	6131	3.3(5)	–	–	–	$(31/2) \rightarrow 27/2^-$
1348.6(0.2)	1349	23(9)	–	0.36(12)	0.06(17)	$11/2^+ \rightarrow 7/2^+$

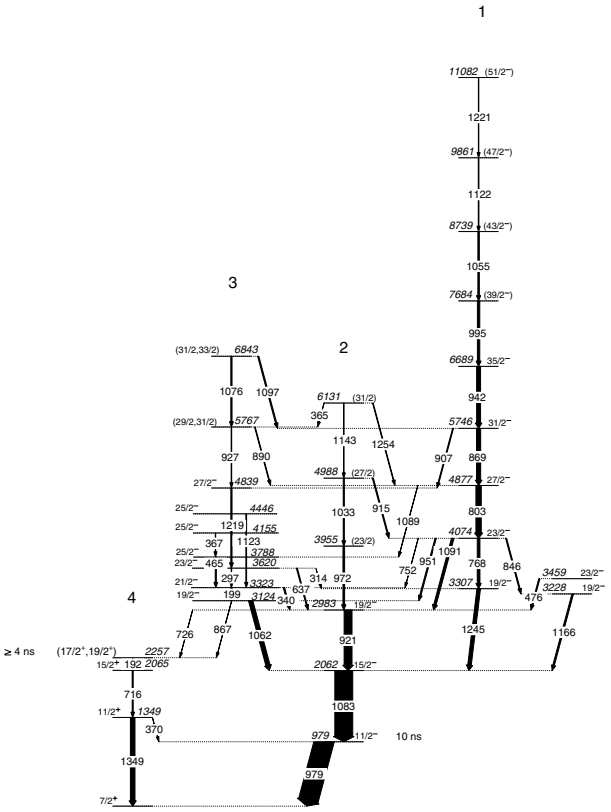

Fig. 9. Level scheme of ^{111}Sn obtained in the ^{98}Mo(^{16}O, 3n) reaction.

3.2.2 Band 2

The g.s. band, previously known up to the $19/2^-$, 2983 keV level [7,17] was extended up to a tentatively introduced $(31/2^-)$, 6131 keV level de-exciting via a sequence of weak 1143, 1033 and 972 keV transitions feeding the 2983 keV level.

3.2.3 Band 3

A second negative-parity sequence (band 3) was known previously [8] up to the $27/2^-$, 4839 keV level. An extension to the $(31/2^-, 33/2^-)$, 6843 keV level is proposed.

3.2.4 Band 4

A cascade of 192($M1$+$E2$)-716($E2$)-1349($E2$) keV transitions (figs. 9 and 10), feeding directly the $7/2^+$ ground state in ^{111}Sn has been found in the coincidence spectra shown in fig. 5. In addition to the known [7] isomeric state at 979 keV, an indication has been found for a new isomer in ^{111}Sn with half-life $T_{1/2} \geq 4$ ns at an excitation energy of 2257 keV. A spin 17/2 or 19/2 is proposed for this isomer. Unfortunately, the 192 keV line is contaminated, therefore only a limit for the half-life of the 2257 keV level could be established. By comparison with the known (remeasured in the present work) isomeric state at 979 keV

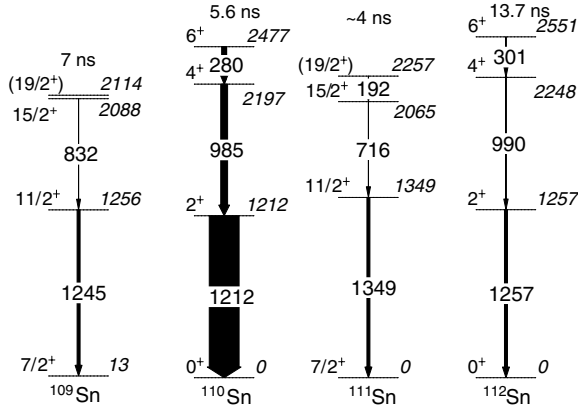

Fig. 10. The $g_{7/2}$ neutron-core coupling in ^{111}Sn and the lowest excited states in the neighbouring nuclei ^{109}Sn, ^{110}Sn and ^{112}Sn (see disscusion in sect. 4.3).

with half-life of about 10 ns, one can conclude that the half-life of the 2257 keV level should be shorter than 10 ns and longer than or equal to 4 ns.

4 Discussion

4.1 Excited states in ^{110}Sn

4.1.1 Low- and medium-spin excitations

Isotopes of tin, accesible now in a range of neutrons from $N = 50$ up to $N = 86$, constitute a paricularly useful set to study the nuclear structure. Along this line one finds two doubly magic nuclei, ^{100}Sn and ^{132}Sn, the very exotic isotopes beyond the $N = 82$ line and the complete set of isotopes in between the two closed neutron shells, $N = 50$ and $N = 82$. It is thus possible to study the evolution of the nuclear structure within the entire shell as a function of the growing neutron number. Moreover, due to the magic proton number of tin isotopes, $Z = 50$, their structure at low energy is expected to be dominated by neutron excitations, corresponding to spherical configurations. This makes the studies of tin nuclei easier and allows more detailed investigations of neutron excitations, than possible in nuclei where both protons and neutrons contribute to excitations.

The ^{110}Sn isotope is located at an interesting point of the discussed neutron line, where the $g_{7/2}$ and $d_{5/2}$ orbitals are nearly filled and the $h_{11/2}$ starts to be occupied. Residing at such transition point makes ^{110}Sn more complex than isotopes, which are a few neutrons to the right or to the left of it. This can be seen in fig. 11, where we show excitations in even-even tin nuclei around ^{110}Sn.

In ^{102}Sn at $N = 52$, one pair of neutrons can form the $\left(g^2_{7/2}\right)_j$ multiplet with maximum spin $j = 6$. At $N = 54$, one pair of neutrons on the $g_{7/2}$ orbital and the other pair on the $d_{5/2}$ orbital can form a multiplet with maximum spin $j = 10$, as observed in ^{104}Sn and heavier tin isotopes. The excitation energy of this 10^+ configuration

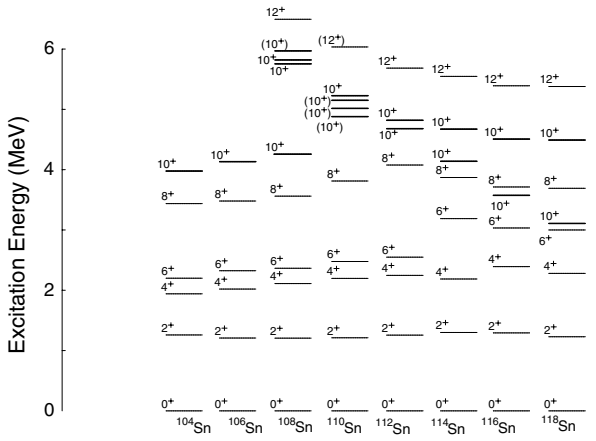

Fig. 11. Systematics of the positive-parity states in even-A Sn isotopes.

grows quickly towards ^{110}Sn, reflecting the fact that both $g_{7/2}$ and $d_{5/2}$ orbitals hide into the core.

Around ^{110}Sn a pair of neutrons starts to populate the $h_{11/2}$ orbital and form a characteristic multiplet $\nu(h^2_{11/2})_j$, with maximum spin $j = 10$. The $I^\pi = 10^+$ states, corresponding to such configuration, are well known in ^{118}Sn and heavier tin isotopes, due to their isomeric character. One sees in fig. 11 that the excitation energy of these 10^+, $h^2_{11/2}$ states decreases with increasing neutron number, as more neutrons are placed in the $h_{11/2}$ shell.

Figure 11 shows that in ^{110}Sn and ^{112}Sn nuclei, members of $\nu(h^2_{11/2})_j$ and $\nu(g^2_{7/2}d^2_{5/2})_j$ multiplets with the same spin approach similar energies. Consequently, the yrast 10^+ excitation, which in ^{104}Sn corresponds to a rather clean $\nu(g^2_{7/2}d^2_{5/2})$ configuration and in ^{118}Sn to a rather clean $\nu h^2_{11/2}$ configuration, in ^{110}Sn may be a mixture of both these configurations and it is expected that there should be two close-lying 10^+ levels in ^{110}Sn. The present work confirms this, reporting more than one 10^+ level in ^{110}Sn. The $\nu(h^2_{11/2})_{10^+}$ excitation in ^{110}Sn was observed at 5227 keV previously [3]. Considering the decay mode of the 5016 keV level and the systematics of fig. 11, we propose that this level corresponds to the $\nu[g^2_{7/2}d^2_{5/2}]_{10^+}$ configuration.

We note that in ^{112}Sn both 10^+ excitations have lower excitation energies than in ^{110}Sn. While for the $\nu(h^2_{11/2})_{10^+}$ excitation this is expected, the $\nu[g^2_{7/2}d^2_{5/2}]_{10^+}$ configuration should appear at higher excitation energy. Another interesting observation made in this work is that in ^{110}Sn there are not two but four 10^+ excitations, close in energy. These two facts indicate that apart from the two-neutron levels there are also other modes excitating 10^+ levels.

Three decades ago, Kleinheinz *et al.* [18] observed a new type of excitation in the $N = 87$ lanthanide nuclei, in which a neutron is promoted from the 11/2[505] orbital of the $h_{11/2}$ parentage intruding from *below* the $N = 82$ closed shell. In such an excitation the occupation of the *upsloping* 11/2[505] orbital decreases. Consequently, the deformation corresponding to such a configuration is larger than that of other configurations in the same nucleus [19]. Shortly afterwards, a similar effect was observed in odd-A ,$^{113-119}$Sb isotopes [20]. Here a proton particle is promoted from the 9/2[404] orbital, intruding from below the $Z = 50$ closed shell, producing deformed $9/2^+$ levels in Sb nuclei. Recently, strongly deformed bands were identified in the mass $A \sim 100$ region [21,22], which correspond to neutron excitation from the 9/2[404] orbital, intruding from below the $N = 50$ closed shell.

We see that the discussed mechanism is rather common and one may expect other types of excitations involving such an upsloping orbital. Indeed, the excitation of a pair of protons from the 9/2[404] orbital to the 1/2[431] orbital of $g_{7/2}$ parentage was observed in $^{112-118}$Sn nuclei [4]. Rotational bands, built on top of these 2p-2h, $[(1/2[431])^2(9/2[404])^{-2}]_{0^+}$ proton configuration, correspond to a moderate deformation in these, otherwise, spherical nuclei. Non-yrast 10^+ levels in $^{112-118}$Sn, shown in fig. 11, were described as members of such 2p-2h bands [4].

Systematics of the discussed 2p-2h bands shown in fig. 7 of ref. [4] indicates that both, the deformation and excitation energies in these bands, do not change rapidly with the neutron number and one may expect such 2p-2h bands also in lighter Sn isotopes. We propose that band 8 shown in fig. 8 corresponds to the $(1/2[431])^2(9/2[404])^{-2}$ proton excitation in ^{110}Sn. Therefore, the 10^+ level at 4880 keV corresponds to such a collective excitation. We note that in fig. 11 the 4880 keV level follows smoothly the systematics of 10^+, 2p-2h excitations, observed in $^{112-118}$Sn isotopes. Low-spin members of 2p-2h bands are not observed in ^{112,114}Sn [4] as these bands decay to the g.s. band before reaching their band heads. The 2p-2h band in ^{114}Sn decays predominantly from the 4^+ band member while in ^{112}Sn from the 6^+ band member. The observation of the decay of the proposed 2p-2h band in ^{110}Sn from the 8^+ band member is consistent with this trend.

It is interesting to note that the alignment of band 8 increases smoothly and is almost parallel to that in band 3; fig. 12, however, shows a tendency for higher placed band crossing. This indicates a band built on a collective excitation mode.

The fourth 10^+ level proposed in ^{110}Sn at 5218 keV may appear thanks to the above-mentioned, higher number of *various* neutron pairs which can be excited in this nucleus, as compared to its neighbours. In particular, one may expect that the $\nu[g^2_{7/2}h^2_{11/2}]_j$ multiplet will compete with the $\nu[g^2_{7/2}d^2_{5/2}]_j$ and $(h^2_{11/2})_j$ multiplets, providing another near-yrast 10^+ excitation.

Due to the same effect there are also more 8^+, near-yrast levels in ^{110}Sn than in its neigbours. The yrast 8^+ level at 3812 keV was observed previously and interpreted as a member of the $\nu[g^2_{7/2}d^2_{5/2}]_j$ multiplet. In the present work we proposed four new 8^+ excitations. The 8^+ level at 4137 keV is a member of the 2p-2h band, as discussed above. The remaining three 8^+ levels are probably due to

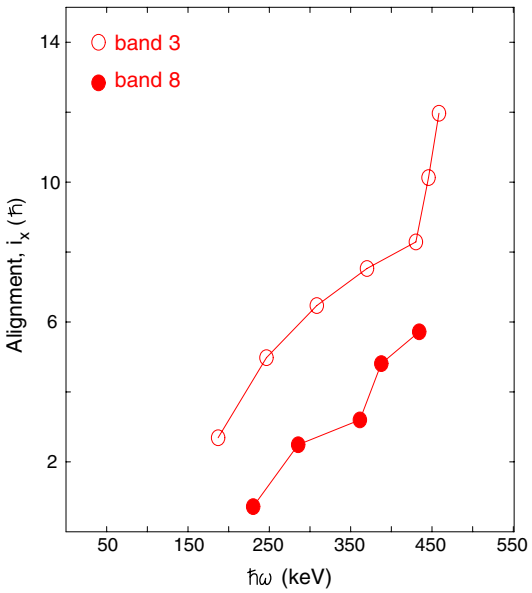

Fig. 12. Aligned angular momenta of band 3 (intruder band) in ^{110}Sn compared with the newly observed collective band 8. A reference configuration with parameters $J_0 = 15\hbar^2\,\mathrm{MeV}^{-1}$ and $J_1 = 25\hbar^4\,\mathrm{MeV}^{-3}$ has been subtracted.

spherical excitations, which may be rather mixed. We note that the 10^+ level at 5227 keV, interpreted as the $h^2_{11/2}$ configuration, decays to the 8^+ proposed at 4314 keV. This suggests that this 8^+ level corresponds to the $(h^2_{11/2})_j$ multiplet. One may also expect near the yrast line two other 8^+ levels, members of $\nu[g^2_{7/2}h^2_{11/2}]_j$ and $\nu[d^2_{5/2}h^2_{11/2}]_j$ multiplets. In an analogous way one may interpret five 6^+, near-yrast levels observed in this work in ^{110}Sn.

Negative-parity excitations in ^{110}Sn were observed previously from spin $I = 7^-$ up [23]. A characteristic excitation with negative parity, observed in Sn isotopes, corresponds to the maximum aligned neutron configuration $(h_{11/2}g_{7/2})_{9^-}$. In ^{110}Sn it is observed at 3931 keV. We note that the $(h^2_{11/2})_{10^+}$ at 5227 decays to this 9^- state, as observed in other Sn isotopes, supporting the presence of the $h_{11/2}$ neutron orbital in both excitations. In this work we also observe low-spin, negative-parity states. The proposed 3^- level at 2458 keV may correspond either to the $(h_{11/2}d_{5/2})_{3^-}$ configuration, with anti-parallel spins or to an octupole phonon coupling, acting between such a pair of $\Delta j = \Delta l$ orbitals.

The energy spacings (fig. 13) between the 9^- and 11^- as well as 11^- and (13^-) states are very close to the energies of the 2^+ and 4^+ states in ^{108}Sn. Thus, the 5106 and 6544 keV states may originate from the fully aligned $\nu(g_{7/2}h_{11/2})_{9^-}$ member of the multiplet coupled to the 2^+ and 4^+ states in ^{108}Sn, respectively. Their experimental energies are quite correctly reproduced in the zeroth-order approximation, *i.e.* by summing of the corresponding level energies. The fact that both states decay via $E2$ transitions further supports the proposed interpretation.

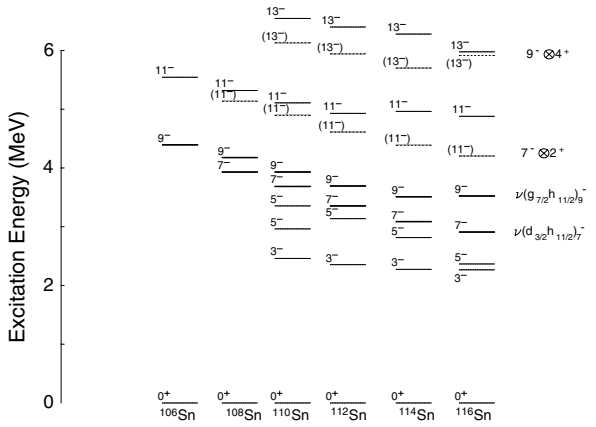

Fig. 13. Systematics of odd-spin, negative-parity states in selected even-A Sn isotopes.

In the ground-state band one observes four-neutron, $\nu[g^2_{7/2}d^2_{5/2}]_{10^+}$ excitations. Therefore, it is expected that negative-parity states could also involve two pairs of neutrons, here $\nu[(h_{11/2}g_{7/2})(d^2_{5/2})]_j$ or $\nu[(h_{11/2}d_{5/2})(g^2_{7/2})]_j$, which may couple to a maximum spin of 13^-. These two configurations can explain the bunch of negative-parity levels in ^{110}Sn marked in fig. 8 as band 1 (we note that in most cases there are two levels with the same spin here).

4.1.2 High-spin excitations

High-spin excitations in tin isotopes can be generated either by exciting additional neutron pairs or by aligning neutrons in the neutron core associated with the 2p-2h deformed proton band. It is likely that both these mechanisms are responsible for the high-spin band in ^{110}Sn (band 3 in fig. 8).

The excitation of various neutron pairs is expected to be particularly visible in ^{110}Sn, where three neutron orbitals, $g_{7/2}$, $d_{5/2}$ and $h_{11/2}$, are near the Fermi level. While in ^{104}Sn the maximum aligned $g^2_{7/2}d^2_{5/2}$ four-neutron configuration provides spin $I = 10$, in ^{110}Sn one may generate spin $I = 16$ placing four neutrons in the $g^2_{7/2}h^2_{11/2}$ configuration. We note that the excitation energy of the 16^+ level at 7586 keV in ^{110}Sn is close to the sum of excitation energies of the $(h^2_{11/2})_{10^+}$ level at 5227 keV and the 2477 keV, 6^+ level of (probable) $g^2_{7/2}$ structure. Continuing this, one might consider the maximum aligned six-neutron configuration $d^2_{5/2}g^2_{7/2}h^2_{11/2}$ with spin $I = 20$ as a member of band 3. There are some arguments against this, however. Such six-neutron configuration level is expected to be spherical, while band 3 looks like a collective structure. An approximate excitation energy of this six-neutron level equals the sum of the 5016 keV, 10^+ level (of likely $g^2_{7/2}d^2_{5/2}$ configuration) and the 5277 keV, $(h^2_{11/2})_{10^+}$ excitation, is significantly higher than the energy of the 20^+ level at 9493 keV. Finally, band 3 continues to still higher spins. All this suggests a collective motion contribution to the structure of band 3.

The 2p-2h deformed configuration in $^{110-118}$Sn was named a "ground-state intruder configuration" [24] to stress that the neutron core in this band corresponds to the ground-state configuration. At high rotational frequencies the neutron ground-state configuration may align. It is expected to happen in tin isotopes with well-populated $h_{11/2}$, high-spin orbital and is indeed seen in ^{112}Sn [24] and ^{114}Sn [25], where a clear backbending in the 2p-2h band is observed around spin $I = 12$. The S-band containing an aligned pair of $h_{11/2}$ neutrons and called in ref. [24] an "aligned intruder configuration", is a continuation of the ground-state 2p-2h band. The picture is, however, different in lighter tin isotopes, where the $h_{11/2}$ orbital is less populated and $g_{7/2}$ and $d_{5/2}$ orbitals are near the Fermi level.

The collective band above the 5227 keV, 10^+ level in ^{110}Sn was observed in refs. [3,24], where it was suggested that it may be analogous to the 2p-2h, aligned intruder configurations seen in heavier tin isotopes. However, the non-observation of the ground-state intruder band in ^{110}Sn, prevented more definite conclusions. The observation of band 8 in ^{110}Sn in the present work allows further discussions.

As seen already by Bron *et al.* [4], the decay of the 2p-2h band to the ground-state configuration in ^{112}Sn differs from that in the heavier tin isotopes. In $^{112-118}$Sn the 2p-2h intruder band has lower excitation energy and, therefore, lower probability to decay out of the band before reaching the band head. The increased binding energy in the 2p-2h band of $^{112-118}$Sn has been attributed to the proton-neutron interaction of the $g_{9/2}$ protons with the $h_{11/2}$ neutrons available for $N \geq 64$ [26]. In ^{112}Sn and in ^{110}Sn the neutron core has contributions from $g_{7/2}$ and $d_{5/2}$ orbitals. Therefore the 2p-2h band has higher excitation energy and decays out of the band to the ground-state, spherical levels coresponding to the $d^2_{5/2}g^2_{7/2}$ excitations. Such a composition of the ground-state intruder band in ^{110}Sn will also cause different alignment than that seen in heavier tin isotopes. In ^{110}Sn all three neutron orbitals may align and the resulting 12^+ aligned state at 6035 keV is expected to contain contributions from the $g_{7/2}$, $d_{5/2}$ and $h_{11/2}$ neutron pairs. This would explain the complex decay pattern of this level. It is still surprising, though, that the aligned 2p-2h band in ^{110}Sn does not decay to the ground-state 2p-2h band in this nucleus. A similar effect was observed in ^{108}Sn [27].

High-spin, negative-parity collective excitations, corresponding to the $(g^{-1}_{9/2}h_{11/2})$ proton excitation across the $Z = 50$ shell were reported in ^{112,114}Sn isotopes [25]. The band head in ^{114}Sn was reported at 4046 keV. In ^{108}Sn the authors of ref. [27] suggest the $(g^{-1}_{9/2}g_{7/2})$ protons coupled to a negative-parity neutron excitation to explain the 6667 keV head of a strongly coupled band in this nucleus. In ^{110}Sn a strongly compressed band is observed starting at 5936 keV. We could not assign parities to this band. Therefore, more experimental work will be required to clear its nature. As discussed above, relevant high-K, particle-hole proton excitations are present in this region, which could explain such a band.

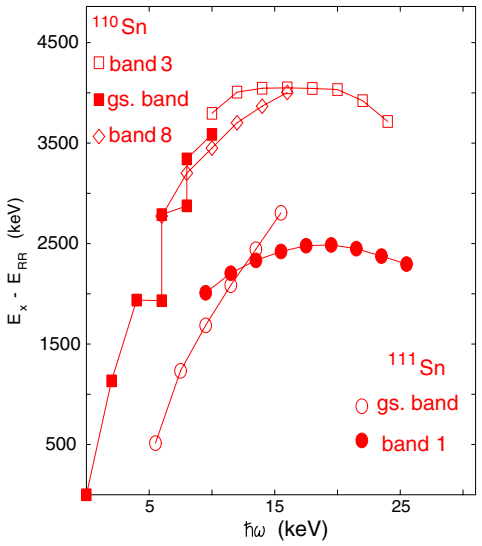

Fig. 14. Rigid rotation-like behaviour of the intruder band in the ^{110}Sn and ^{111}Sn, nuclei relative to rigid rotor reference. A reference configuration with parameters $J_0 = 15\hbar^2\,\mathrm{MeV}^{-1}$ and $J_1 = 25\hbar^4\,\mathrm{MeV}^{-3}$ has been also subtracted.

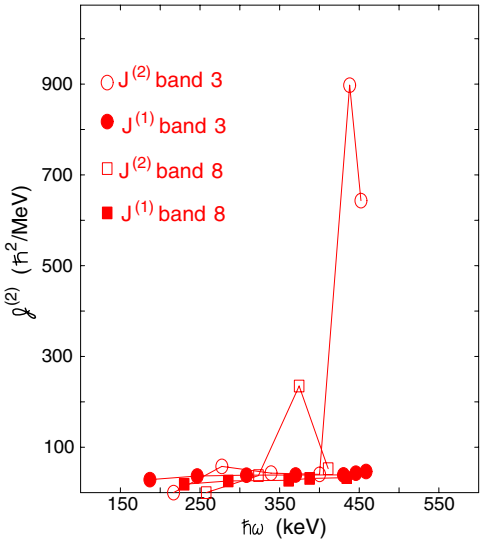

Fig. 15. Experimental kinematic $J^{(1)}$ and dynamic $J^{(2)}$ moments of inertia for band 3 shown in ^{110}Sn. The $J^{(2)}$ irregular function of rotational frequency typical for the rigid rotation-like band termination is shown.

4.1.3 Unsmooth band termination in ^{110}Sn nucleus

The dynamic moment of inertia $J^{(2)}$ is a very sensitive measure of any structural changes taking place within a band. A smooth character of $J^{(2)}$ can be considered as a sign that the band remains pure up to the termination point (*e.g.* ^{109}Sb [28]).

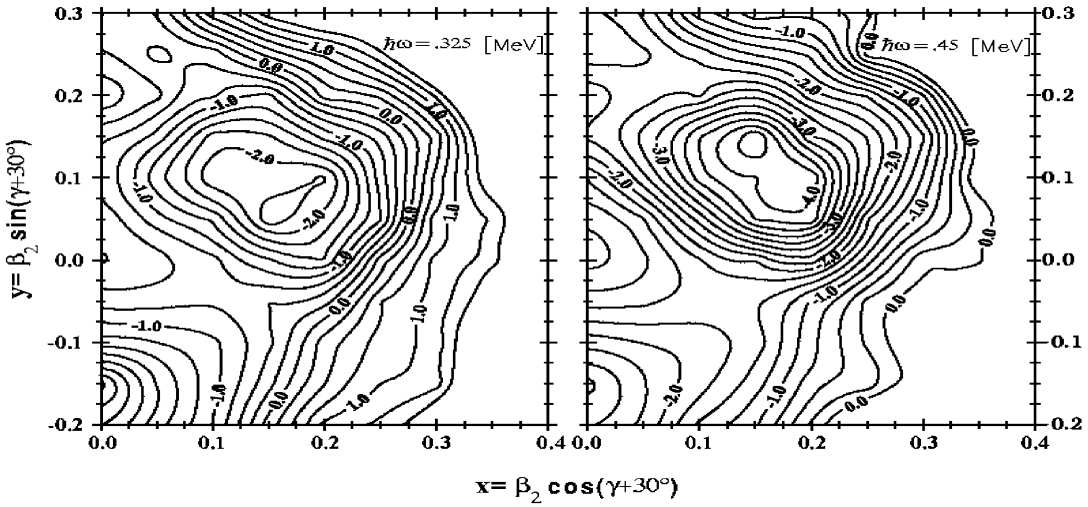

Fig. 16. Total Routhian surfaces calculated for ^{110}Sn at the frequencies $\hbar\omega = 0.325\,\mathrm{MeV}$ and $\hbar\omega = 0.45\,\mathrm{MeV}$, *i.e.* before and after neutron alignment, respectively. The distance between the contour lines is 250 keV.

When $J^{(2)}$ of an observed band is an irregular function of rotational frequency in the vicinity of band termination, the description *unsmooth band termination* is used [28]. An example of such unsmoothly terminating band seems to be band 3 (in fig. 8) of ^{110}Sn, shown in figs. 14 and 15 and classified as a case of rigid rotation-like band termination [28]. The disturbance of the smoothness might be caused by several reasons, *i.e.* the terminating structure might cross with some other more collective configuration and/or other configurations which terminate at lower spin values may come close in energy and thus interact with the states of the band approaching termination.

4.2 Excited states in the nucleus ^{111}Sn

An extention of the g.s. band above the $19/2^-$, 2983 keV state is weakly developed and the spin-parity assignments for the 3955, 4988 and 6131 keV levels is still an open question. The levels might have positive parities as was observed in ^{115}Sn [29]. In such case, these states could arise from the $h^2_{11/2}g_{7/2}$ multiplet.

The deformed intruder band in ^{111}Sn which was proposed [7] to originate from the $\nu h_{11/2}$ orbital coupled to the deformed proton 2p2h excitation across the $Z = 50$ shell gap, is also observed in the present experiment. The configuration proposed for this structure is $\nu h_{11/2} \otimes [(\pi g_{7/2})^2(\pi g_{9/2})^{-2}]$ [7] or $\nu h_{11/2} \otimes [\pi(g_{7/2}d_{5/2})(g_{9/2})^{-2}]$ [30]. This band develops on top of the $23/2^-$ state at 4074 keV, corresponding to a configuration $\nu h_{11/2} \otimes 6^+$ [7]. It decays to at least four $19/2^-$ states arising from coupling of the $h_{11/2}$ neutron to admixtures of the spherical and deformed 4^+ and 6^+ states in ^{110}Sn.

The negative-parity band 3 may originate from the $h_{11/2}$ orbital coupled to the 4^+, 6^+, 8^+ and 10^+ states in ^{110}Sn. The 3124 keV state can be interpreted as a fully aligned member of the $\nu h_{11/2} \otimes 4^+$ multiplet. The maximum spin state from the $\nu h_{11/2} \otimes 10^+$ configuration is $31/2$ which may be assigned to the 6843 keV state.

The nature of the 2257 keV, possibly an isomeric state, can be explained if one assumes that the observed levels in ^{111}Sn result from the coupling of the $g_{7/2}$ neutron to the closed neutron shell excitations of the $^{110}_{50}\mathrm{Sn}_{60}$ core nucleus (fig. 10). Therefore, one can expect that the 192 keV transition in ^{111}Sn should be of the same nature as the 280 keV transition occurring between the 6^+_1 and 4^+_1 states in ^{110}Sn. Hence, one can expect the 192 keV isomeric transition in ^{111}Sn to be a hindered $E2$ one. Since the $g_{7/2}$ neutron is a spectator, the reduced transition probability $B(E2; 19/2^+ \rightarrow 15/2^+)$ is proportional to $B(E2; 6^+ \rightarrow 4^+)$. Therefore the half-life of the 2257 keV, $19/2^+$ state in ^{111}Sn can be deduced from the half-life of the 6^+ state in ^{110}Sn by taking into account the energy dependence of $T_{1/2}$. The 6^+ state in ^{110}Sn has a half-life of 5.6 ns [4], which gives for the 2257 keV level in ^{111}Sn a lifetime of 37 ns, which is approximately an order of magnitude larger than the experimental value. The enhancement of the 192 keV transition ($B(E2; (19/2)^+ \rightarrow 15/2^+) = 263\ e^2\,\mathrm{fm}^2$) in comparison with the 280 keV transition ($B(E2; 6^+ \rightarrow 4^+) = 29\ e^2\,\mathrm{fm}^2$) can possibly be explained by the polarization effect. The neutron coupled to the excited core can polarize the latter and influence the effective charge, e_{eff}, which can result in an increase of the $E2$ transition probability.

4.3 TRS calculations and comparison with experimental data

In order to gain a better understanding of the band structure observed in experiment, Self-Consistent Total-Routhian-Surface (SC-TRS) calculations have been performed. The total Routhian was minimised on a lattice in the (β_2, γ) space with hexadecapole deformation β_4 included in the calculation. The deformed Woods-Saxon

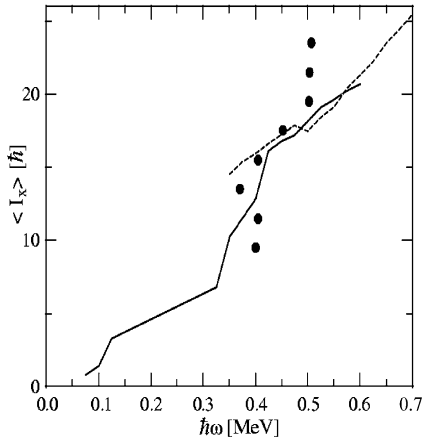

Fig. 17. The calculated (solid $\gamma < 0$ and dashed $\gamma > 0$ lines) and experimental (dots) values of the total angular momentum as a function of rotational frequency in ^{110}Sn.

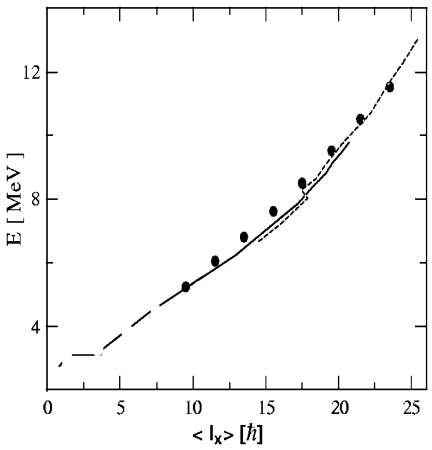

Fig. 18. The calculated (solid $\gamma < 0$ and dashed $\gamma > 0$ lines) and experimental (dots) excitation energies as a function of total angular momentum in ^{110}Sn.

potential with a new set of parameters adapted and incorporated into the TRS program by R. Wyss was used as a single-particle potential. For a detailed description of this model see refs. [31,32] and references quoted therein. Examples of TR surfaces for the yrast configuration in ^{110}Sn are shown in fig. 16.

The results of the calculations suggest a quadrupole deformation with the deformation parameters $\beta_2 \approx 0.2$ and $\gamma \approx -5°$ for the yrast band (band 3) at rotational frequencies $\hbar\omega \leq 0.35$ ($I_x < 14\ \hbar$). However, the experimental data suggest that the levels in this region of excitation energies have not a pure rotational nature. Above the alignment of the $h^2_{11/2}$ neutrons at $\hbar\omega > 0.35$ MeV the TRS calculations predict that the shape of the nucleus becomes triaxial (with $\gamma \approx 15°$), but that the deformation parameter β_2 does not change. The 2-quasi-neutron $h^2_{11/2}$ configuration drives the nucleus towards a positive γ deformation, so, one can conclude that the angular-momentum alignment (due to aligned neutrons) will influence significantly the evolution of the shape.

The calculated angular momenta and excitation energies are compared with the experimental data in figs. 17 and 18, respectively.

One observes a satisfactory good agreement between calculated and experimental data until $\hbar\omega = 0.5$, where distinct discrepancies appear. However, the plot of the total energy as a function of angular momentum, fig. 18, does not exhibit such a discrepancy.

In the case of ^{111}Sn, the calculations predict a prolate shape of the nucleus with a quadrupole deformation β_2 between 0.18 and 0.2 and γ between $-2.3°$ and $-5°$.

5 Summary

Excited states in ^{110}Sn, ^{111}Sn and in neighbouring nuclei have been investigated in the ^{98}Mo + ^{16}O reaction using the OSIRIS-II Ge detector array equipped with the multiplicity filter.

The results are:

- Main γ-ray branches feeding the 6^+, 2477 keV isomer of the g.s. band in ^{110}Sn are confirmed based on coincidence relations, angular-distribution measurements and relative excitation function data. Four new levels on the top 6^+ isomer state are proposed up to spin 10^+ (band 5).
- The newly proposed band 2 showing most likely $\Delta I = 1$ structure is introduced into the level scheme of ^{110}Sn.
- The intruder band in ^{110}Sn (band 3) based on the deformed 2h-2p configuration is extended to higher spins by $(22^+) \rightarrow (20^+)$ and $(24^+) \rightarrow (22^+)$ transitions. The nature of newly introduced 10^+ states fed in the decay of the collective band is discussed.
- New positive-parity bands 4 and 6 in ^{110}Sn based on $\nu g^2_{7/2}$ and $\nu(d^2_{5/2}g^2_{7/2})$ spherical states, strongly connected to the g.s. band, are introduced.
- A bunch of levels labeled as band 7 is introduced based on coincidence relations of γ-rays which correspond with 2^+ and/or 4^+ states in the g.s. band.
- A new sequence of levels labeled as band 8 showing rotational-like behaviour is proposed.
- The negative-parity band in ^{110}Sn was extended to its low-spin part. The 3^- and 5^- states are proposed.
- It is argued that the newly established in ^{111}Sn cascade of $(19/2, 17/2)^+ \rightarrow 15/2^+ \rightarrow 11/2^+ \rightarrow 7/2^+$ transitions results from a $g_{7/2}$ neutron coupled to the ^{110}Sn core.
- The negative-parity bands in ^{111}Sn are extended to higher spins.
- An attempt was made to provide an experimental fingerprint to classify an observed excited band as a shape coexisting by deducing experimental $B(E2)$ γ-ray branching ratios between the intruder and yrast states in the nuclei ^{110}Sn, ^{111}Sn and ^{112}Sn. The presence of strong intraband $B(E2)$ values and hindered interband decays is found, which is one of the important fingerprints.

We are very grateful to the staff of the Heavy Ion Laboratory at the Warsaw University for providing excellent beam conditions and for all support at each stage of the work. The work was financially supported by the Polish Committee for Scientific Research (grants KBN No. 2 P03B-02308 and No. 5 P03B 03620).

References

1. K. Heyde, J. De Beule, B. Decroix, C. De Coster, A.M. Oros, CERN-EP/ **98-181**, 1 (1998).
2. M. Singh, J.W. Sunier, R.M. Devries, G.E. Thompson, Nucl. Phys. A **193**, 449 (1972).
3. D.A. Viggars, H.v. Taylor, B. Singh, J.C. Vaddington, Phys. Rev. C **36**, 1006 (1987).
4. J. Bron, W.H.A. Hesselink, A. van Poelgeest, A.J.J. Zalmstra, J.M. Uitzinger, H. Verheul, Nucl. Phys. A **318**, 335 (1979).
5. F. Azaiez, S. Andriamonje, J.F. Chemin, M. Fidah, J.N. Scheurer, M.M. Alèonard, G. Bastin, J.P. Thibaud, F. Beck, G. Costa, J.F. Bruandet, F. Litard, Nucl. Phys. A **501**, 401 (1989).
6. R. Wadsworth, H.R. Andrews, R.M. Clark, D.B. Fossan, A. Galindo-Uribarri, J.R. Hughes, V.P. Janzen, D.R. LaFosse, S.M. Mullins, E.S. Paul, D.C. Radford, H. Schnare, P. Vaska, D. Ward, J.N. Wilson, R. Wyss, Nucl. Phys. A **559**, 461 (1993).
7. D.R. LaFosse, D.B. Fossan, J.R. Hughes, Y. Liang, P. Vaska, M.P. Waring, J.-Y. Zhang, Phys. Rev. C **51**, R2876 (1995).
8. V.P. Janzen, Phys. Scr. **T56**, 144 (1995).
9. M.E.J. Wigmans, R.J. Heynis, P.M.A. van der Kam, H. Verheul, Phys. Rev. C **14**, 229 (1976).
10. P.J. Blankert, H.P. Blok, J. Blok, Nucl. Phys. A **356**, 74 (1981).
11. J.L. Wood, K. Heyde, W. Nazarewicz, M. Huyse, P. Van Duppen, Phys. Rep. **215**, 101 (1992).
12. P. Kowina, *High spin states in* ^{110}Sn, MSc Thesis, 1999.
13. M. Wolinska-Cichocka, B. Bekman, Ch. Droste, J. Dworski, W. Gast, J. Iwanicki, H. Jäger, M. Kisieliński, A. Kordyasz, M. Kowalczyk, J. Kownacki, R. Lieder, W. Męczyński, T. Morek, M. Palacz, J. Perkowski, E. Ruchowska, J. Srebrny, A. Stolarz, J. Styczeń, Acta Phys. Pol. B **34**, 2305; 2309 (2003).
14. D.C. Radford, Nucl. Instrum. Methods A **236**, 297 (1995).
15. G.M. Crawley, W. Benenson, G. Bertsch, S. Gales, D. Weber, B. Zwięgliński, Phys. Rev. C **23**, 589 (1981).
16. P.M. Endt, At. Data Nucl. Data Tables, **26**, 47 (1981).
17. G. Gangopadhyay, A.K. Singh, D. Banerjee, R. Bhattacharya, R.K. Bhownik, S. Muralithar, G. Rodriguez, R.P. Singh, A. Goswami, S. Bhattacharya, B. Dasmahapatra, S. Sen, Z. Phys. A **351**, 1 (1995).
18. P. Kleinheinz, R.K. Sheline, M.R. Maier, R.M. Diamond, F.S. Stephens *et al.*, Phys. Rev. Lett. **32**, 68 (1974).
19. P. Kleinheinz, A.M. Stefanini, M.R. Maier, R.K. Sheline, R.M. Diamond, F.S. Stephens Nucl. Phys. A **283**, 189 (1977).
20. A.K. Gaigalas, R.E. Shroy, G. Schatz, D.B. Fossan, Phys. Rev. Lett. **35**, 555 (1975).
21. W. Urban, J.A. Pinston, T. Rzaca-Urban, A. Złomaniec, G. Simpson, J.L. Durell, W.R. Phillips, A.G. Smith, B.J. Varley, I. Ahmad, N. Schulz, Eur. Phys. J. A **16**, 11 (2003).
22. W. Urban, J.A. Pinston, J. Genevey, T. Rząca-Urban, A. Zlomaniec, G. Simpson, J.L. Durell, W.R. Phillips, A.G. Smith, B.J. Varley, I. Ahmad, N. Schulz, Eur. Phys. J. A **22**, 241 (2004).
23. A. Van Poelgeest, J. Bron, W.H.A. Hesselink, K. Allaart, J.J.A. Zalmstra, M.J. Uitzinger, H. Verheul, Nucl. Phys. A **346**, 70 (1980).
24. H. Harada, T. Murakami, T. Inamura, K. Yoshida, J. Kasagi, T. Kudo, Phys. Lett. B **207**, 17 (1988).
25. M. Schimmer, S. Albers, A. Dewald, A. Gelberg, R. Wirowski, P. von Brentano, Nucl. Phys. A **539**, 527 (1992).
26. K. Heyde, P. Van Isacker, M. Waroquier, J.L. Wood, R.A. Meyer, Phys. Rep. **102**, 291 (1983).
27. S. Juutinen, E. Mäkelä, R. Julin, M. Piiparinen, S. Törmänen, A. Virtanen, E. Adamides, A. Ataç, J. Blomqvist, B. Cederwall, C. Fahlander, E. Ideguchi, A. Johnson, W. Karczmarczyk, J. Kownacki, S. Mitarai, L.-O. Norlin, J. Nyberg, R. Schubart, D. Seweryniak, G. Sletten, Nucl. Phys. A **617**, 74 (1997).
28. A.V. Afanasjev, D.B. Fossan, G.J. Lane, I. Ragnarsson, Phys. Rep. **322**, no. 1 (1999).
29. A. Savelius, S. Juutinen, K. Helariutta, P. Jones, R. Julin, P. Jämsen, M. Muikku, M. Piiparinen, J. Suhonen, S. Törmänen, R. Wyss, P.T. Greenlees, P. Simecek, D. Cutoiu, Nucl. Phys. A **637**, 491 (1998).
30. R. Wadsworth, C.W. Beusang, M. Gromaz, J. DeGraaf, T.E. Drake, D.B. Fossan, S. Flibotte, A. Galindo-Uribari, K. Hauschild, G. Hackman, J.R. Hughes, V.P. Janzen, D.R. LaFosse, S.M. Mullins, E.S. Paul, D.C Radford, H. Schnare, P. Vaska, D. Ward, J.N. Wilson, I. Ragnarsson, Phys. Rev. C **53**, 2763 (1996).
31. W. Satuła, R. Wyss, Phys. Scr. **T56**, 159 (1995).
32. K. Starosta, Ch. Droste, T. Morek, J. Srebrny, D.B. Fossan, D.R. LaFosse, H. Schnare, I. Thorslund, P. Vaska, M.P. Waring, W. Satuła, S.G. Rohoziński, R. Wyss, I.M. Hilbert, R. Wadsworth, K. Hauschild, C.W. Beausang, S.A. Forbes, P.J. Nolan, E.S. Paul, Phys. Rev. C **53**, 137 (1996).